Available online at www.sciencedirect.com

ScienceDirect

Physics Procedia 83 (2016) 882 – 890

Physics Procedia

9th International Conference on Photonic Technologies - LANE 2016

Influence of powder bed preheating on microstructure and mechanical properties of H13 tool steel SLM parts

R. Mertens[a,*], B. Vrancken[b], N. Holmstock[a], Y. Kinds[a], J.-P. Kruth[a], J. Van Humbeeck[b]

[a]KU Leuven, Department of Mechanical Engineering, Celestijnenlaan 300 box 2420, 3001 Leuven, Belgium
[b]KU Leuven, Department of Materials Engineering, Kasteelpark Arenberg 44 box 2450, 3001 Leuven, Belgium

Abstract

Powder bed preheating is a promising development in selective laser melting (SLM), mainly applied to avoid large thermal stresses in the material. This study analyses the effect of in-process preheating on microstructure, mechanical properties and residual stresses during SLM of H13 tool steel. Sample parts are produced without any preheating and are compared to the corresponding parts made with preheating at 100°, 200°, 300°, and 400°C. Interestingly, internal stresses at the top surface of the parts evolve from compressive (-324MPa) without preheating to tensile stresses (371MPa) with preheating at 400°C. Nevertheless, application of powder bed preheating results in a more homogeneous microstructure with better mechanical properties compared to H13 SLM parts produced without preheating. The fine bainitic microstructure leads to hardness values of 650-700Hv and ultimate tensile strength of 1965MPa, which are comparable to or even better than those of conventionally made and heat treated H13 tool steel.

Peer-review under responsibility of the Bayerisches Laserzentrum GmbH

Keywords: Selective laser melting; powder bed preheating; H13 tool steel

1. Introduction

Selective laser melting (SLM) is an additive manufacturing technique in which metal powder is molten by a laser in a layer-by-layer fashion. Its applications mainly consist of complex parts and low-quantity production. Because of the local heating and cooling of the material during the production process, several problems arise such as thermally

* Corresponding author. Tel.: +32-16-37-73-21 .
E-mail address: raya.mertens@kuleuven.be

Peer-review under responsibility of the Bayerisches Laserzentrum GmbH
doi:10.1016/j.phpro.2016.08.092

induced stresses in the parts and formation of inhomogeneous microstructures. One way to overcome these problems consists of in-process powder bed preheating, as mentioned by Gu et al. (2012) and illustrated by Kempen et al. (2014), Vrancken et al. (2015) and Sander et al. (2016).

Powder bed preheating is applied for H13 tool steel. This hot-working tool steel has high hardenability and wear resistance, good thermal fatigue performance and retains toughness and strength at high temperatures, which makes it suitable to be used in tools for hot working operations such as plastic injection molding, die casting, forging and extrusion. Recent studies focus on surface hardening (Telasang et al. (2014b), Zhang et al. (2007), Cong et al. (2014), Jia et al. (2015) and Lee et al. (2009)) and laser cladding (Ouyang et al. (2002), Cottam and Wang (2014), Maziasz et al. (1998), Pinkerton and Li (2005), Telasang et al. (2014), Gu et al. (2012)) of this material. In addition, Cornier et al. (2003) report about the processing of H13 tool steel by electron beam melting, AlMangour et al. (2016) about SLM of H13 and McHugh et al. (2008) about spray forming of H13. All these processes are characterized by rapid cooling of the material and therefore a very fine cellular dendritic microstructure is formed which mainly consists of martensite with retained austenite and carbides at grain boundaries. McHugh et al. (2008) and Eser et al. (2016b) also report formation of bainite during cooling or during tempering of the retained austenite.

In laser hardening, only the top layer of the part is modified and thus hardened. Cong et al. (2014) and Jia et al. (2015) report hardnesses of the top layer between 600 and 700Hv. Telasang et al. (2014b) even obtained hardness values up to 770Hv. During laser cladding, the entire part is made in a similar way and hardness values of 550-650Hv are obtained by Ouyang et al. (2002), Cottam and Wang (2014) and Telasang et al. (2014). Pinkerton and Li (2005) even report hardnesses in the range of 670-770Hv. During laser cladding however, bottom layers undergo a specific thermal history of reheating during deposition of every subsequent layer. Therefore a tempered microstructure is examined in laser cladded H13 parts by Ouyang et al. (2002) and Maziasz et al. (1998). This tempering causes a significant reduction in hardness since the martensite breaks down (Cottam and Wang (2014) and Pinkerton and Li (2005)) into a tempered microstructure.

The martensitic transformation during fast cooling of this material has, besides hardness, also a major influence on internal stresses in the parts. Gu et al. (2012) state that the martensitic transformation leads to volume increases of up to 4%, which induce compressive stresses at the surface of the part. Jia et al. (2015) measured a compressive stress of -170MPa after surface hardening. Cottam and Wang (2014) and Telasang et al. (2014) obtained compressive stresses of respectively -250 and -280MPa in laser cladding. Furthermore, Cottam and Wang (2014) determined stress levels throughout the entire part and concluded that, although compressive stresses are found at the outer surface, tensile stresses (150MPa) are present in the middle of the part which can be explained by the volume decrease during tempering of the martensitic structure. McHugh et al. (2008) obtained similar trends in spray formed parts. Here stress levels were higher in general (ranging from -800MPa compressive stress to 740MPa tensile stress).

So far, the specific microstructure and properties formed by additive manufacturing of this H13 tool steel have been reported extensively. However, none of these studies examine the effect of in-process preheating on microstructure or internal stress levels. In this study, parts produced by SLM without and with preheating temperatures of 100°C, 200°C, 300°C and 400°C are compared. Without application of preheating, the top area of the part consists of a very hard martensitic structure that is largely tempered when moving away from the top surface. This microstructural difference leads to large compressive stresses at the top area. Preheating of 400°C on the other hand leads to a uniform bainitic structure which results in better mechanical properties in comparison to the tempered martensitic structure of parts produced without preheating.

2. Materials and method

The chemical composition of the H13 powder used is listed in Table 1. The powder is produced by gas atomization. Fig. 1 shows the morphology and gives an indication of the size range of the powder particles.

Table 1. Chemical composition of H13 tool steel.

Element	Fe	C	Cr	Mo	Si	V
Weight percentage	≥ 90.95	0.32 – 0.4	5.13 – 5.25	1.33 – 1.4	1	1

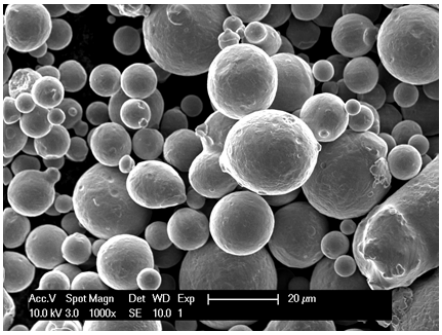

Fig. 1. Gas atomized H13 tool steel powder.

The powder is processed by using an in-house developed SLM-machine of KU Leuven equipped with a Yb:YAG fiber laser with a maximum output power of 300W and a beam diameter d_{1/e^2} of 50µm. Base plate preheating is applied using a resistive heating element underneath the base plate. The temperature is controlled within ± 0.5°C using a thermocouple attached to the heating element and a PID control loop. Since the maximal part height was 10mm and because of the good conductivity of the solid metal, a sufficient homogeneous temperature distribution in the parts during the process is expected. All parts (10x10x10mm³ cubes and tensile specimens) are built by applying a bidirectional scanning strategy with 90° rotation between layers. The layer thickness and scan spacing values were kept constant at 30µm and 105µm respectively. Two parametersets, resulting from the parameter optimization, are used. They both apply a laser power of 170W. Scanning speeds are 400mm/s (parameter set 1) and 800mm/s (parameter set 2). Relative densities are >99% as determined by pixelcount measurements using ImageJ software.

Microstructures and fracture surfaces are inspected by using a Philips XL30 FEG scanning electron microscope. Sample preparation for microstructure images consists of polishing down to OPS and etching with a 2% Nital solution. Phases present in the material are analysed based on XRD diffraction patterns measured with a Siemens D500 goniometer with Cu radiation on polished samples produced with parameter set 2.

Residual stresses at the top surfaces of parts produced with parameter set 1 are determined with the help of XRD stress measurements on a Seifert MZ IV goniometer with Cr radiation. Herefore, the Fe-α {211} peak was scanned which is located around 156.1°. The elastic constants $S_1 = -1.272\text{x}10^{-6}$ MPa^{-1} and $S_2/2 = 7.036\text{x}10^{-6}$ MPa^{-1} (obtained from Costa et al. (2008)) are used.

Vickers microhardnesses are measured using a Future Tech FV-700 hardness tester with an indentation load of 0.5kg on polished surfaces of the parts used for stress measurements. To assess variations of hardness across a section parallel to the building direction, a matrix of hardness measurements is performed (analogous to Cottam and Wang (2014)). The distances from the boarder of the part and between adjacent indentations is fixed at 0.5mm (and in accordance to ASTM E384). In order to obtain accurate hardness values close to the top surface of the parts, hardness measurements are performed on a polished cross section perpendicular to the building direction.

Tensile beam-shape (3x90x10mm³) specimens are produced using parameter set 2 and are machined to final shape by electrical discharge machining. Tensile tests are performed by using an Instron 4505 machine according to ASTM E 8M with a strain rate of 1mm/min.

3. Results

Fig. 2 shows an SEM image of a side view (section along the building direction) of a part produced with parameter set 2 without application of preheating. The building direction is situated towards the top of the figure as indicated by the arrow. A fine cellular structure is observed, which is in accordance to literature. No clear differences in cellular structure are found between parts produced at different preheating temperatures. Differences in microstructures might appear inside of the observed cells. In order to assess this, however, more in depth analysis is necessary.

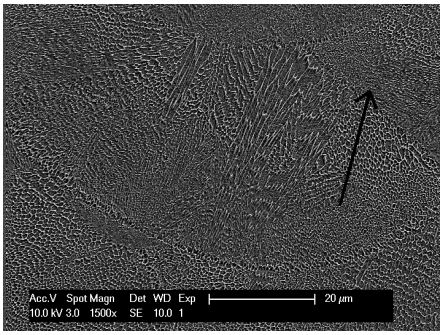

Fig. 2. Side view microstructure without preheating. The arrow indicates the building direction.

XRD spectra of parts produced at three preheating temperatures (Fig. 3) show that both fcc and bcc phases are present for all preheating temperatures. At a preheating temperature of 200°C, bcc is less present compared to production without and at 400°C preheating. 400°C preheating results in the smallest fcc peaks. The fcc peaks indicate the presence of retained austenite in the material. Therefore, there is more retained austenite present in the parts produced at a preheating temperature of 200°C. The bcc peaks represent martensite, but also bainite, since both consist of a distorted bcc (bct) structure.

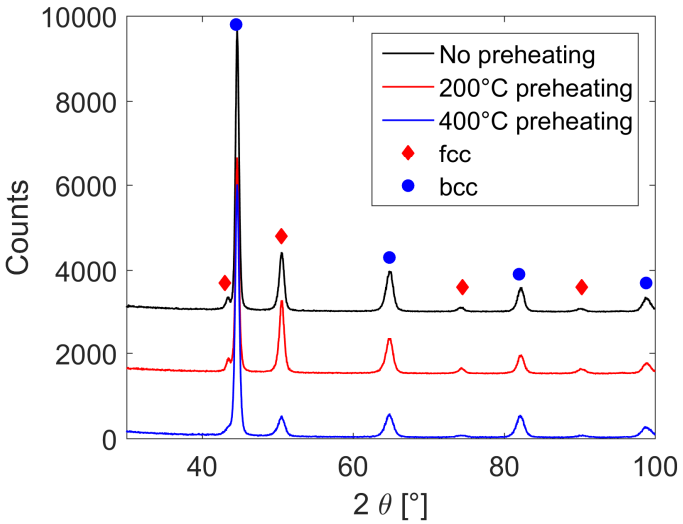

Fig. 3. XRD diffraction patterns for parts produced without and with preheating of 200°C and 400°C.

The residual stress measurements on the top surfaces, performed by XRD, are summarized in Fig. 4. Normal, as well as shear stresses are present in the parts. Fig. 4 shows maximum principal stresses, which allows for a comparison of the largest stress present in each part. Without application of preheating, large compressive stresses are found because of the volume increase during martensite formation, as reported in literature. Increasing the preheating temperature leads to gradually increasing stresses, which become tensile for 300°C and 400°C preheating. During production without preheating, base plate temperatures easily reach 80-90°C. Therefore, the maximum stress level increases approximately linear with preheating temperature from -332MPa at a temperature of about 85°C to 375MPa at a temperature of 400°C.

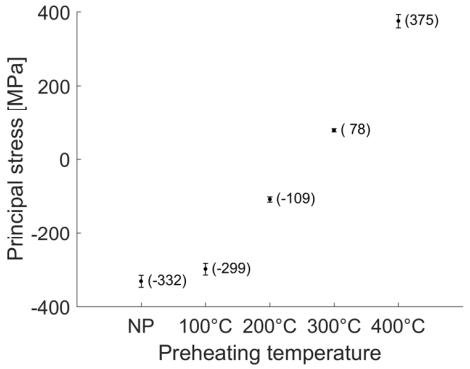

Fig. 4. Residual stress measurements on samples with different preheating temperatures.

Hardness maps of three parts that were used for residual stress measurements are shown in Fig. 5. Each time, a cross section along the building direction is made in the middle of the part. Top surfaces are situated at the top of the images. Each square indicates one indentation. White squares are shown at places where no valid measurement result could be obtained. Dark blue squares indicate very low hardness values, which can be explained by porosities in the parts. In general, preheating at 200°C results in lower overall hardness and preheating of 400°C results in higher overall hardness.

In addition to these measurements, hardness measurements are performed at sections perpendicular to the building direction, close to the top surface of the parts (Table 2). These measurements are carried out because a distance of 500µm from the top surface of the parts was taken into account for the hardness maps. Hardness values at the top layer are very high for parts produced without preheating. This trend is also slightly shown in Fig. 5 where the top row of the part without preheating already shows higher hardness values than the rest of the part. Preheating at 200°C leads to the same trend, but more attenuated. For preheating at 400°C, hardness values of the top layer are similar to the hardnesses obtained in the top 4mm of the part.

The high hardness values obtained at the top of the parts for parts produced without and with 200°C preheating are related to the formation of martensite in each newly solidified layer because of the relatively fast quenching. The significant drop in hardness when moving away from the top surface indicates significant tempering of the martensitic microstructure. For parts produced with a preheating temperature of 400°C however, hardness values are lower in the top layer, but don't drop that fast when moving away from the top surface. Here a more uniform microstructure is formed that suffers less from tempering. In this part, a less pronounced tempering effect is noticed towards the bottom of the part, as can be seen in Fig. 5.

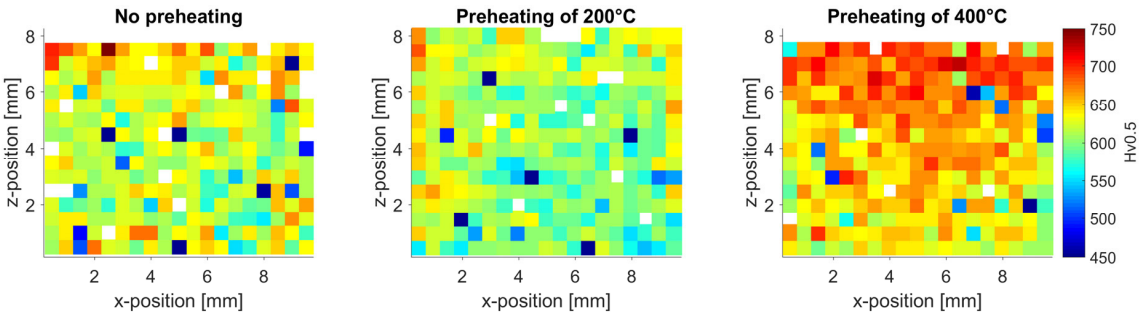

Fig. 5. Vickers microhardness measurements on cross sections for different preheating temperatures. All figures use the same scale.

Table 2. Vickers microhardness values close to the top surface of the parts for different preheating temperatures.

Preheating temperature	No	200°C	400°C
$Hv_{0.5}$ (95% confidence intervals based on 4 measurements)	894 ± 48	706 ± 147	667 ± 83

Finally, tensile properties of the parts produced with different preheating temperatures are assessed. The results of these tensile tests are shown in Fig. 6 and Table 3. First of all, the obtained data show good repeatability. Secondly, significant differences are noticable between different preheating temperatures. Yield and ultimate strength values first decrease and then increase again with increasing preheating temperature. Average elongation at break is similar for all tested preheating temperatures. Important to notice is the significant hardening behavior and high ultimate tensile strength of parts produced with 400°C preheating temperature. The strength obtained here is comparable to conventionally made and heat treated H13 tool steel. This implies that production with preheating can eliminate strengthening post heat treatments. It should be noted however, that elongation at break for the SLMed parts are significantly lower than for conventional material.

Fehler! Verweisquelle konnte nicht gefunden werden. shows fracture surfaces of the different parts. The dimpled structure indicates ductile fractures. All fracture surfaces show lines of porosities, which can explain the low ductility of the parts.

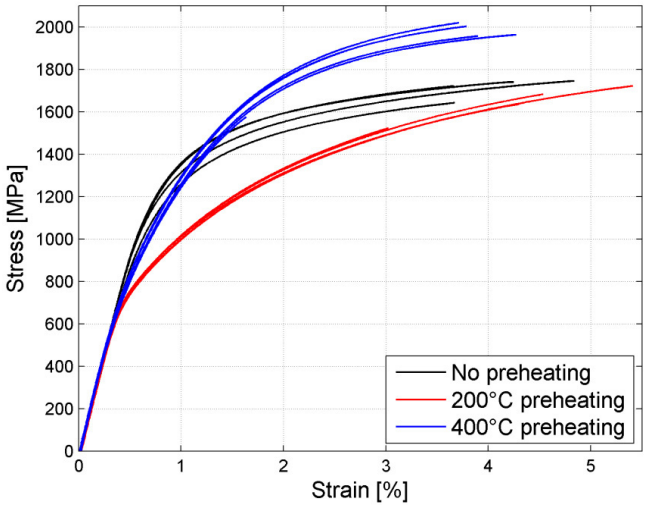

Fig. 6. Stress strain curves for samples without, with 200°C and with 400°C preheating.

Table 3. Summary of tensile tests of specimens produced with different preheating temperatures (95% confidence intervals based on 6 measurements are shown). The comparison with conventionally produced and heat treated H13 tool steel is made.

	Young's Modulus [GPa]	Yield Strength [MPa]	Ultimate Tensile Strength [MPa]	Elongation at break [%]
Conventional	210	1650	1990	9
SLM – no preheating	190 ± 11	1236 ± 178	1712 ± 103	4.1 ± 1.2
SLM – preheating of 200°C	188 ± 5	835 ± 23	1620 ± 215	4.1 ± 2.3
SLM – preheating of 400°C	194 ± 9	1073 ± 72	1965 ± 145	3.7 ± 1.7

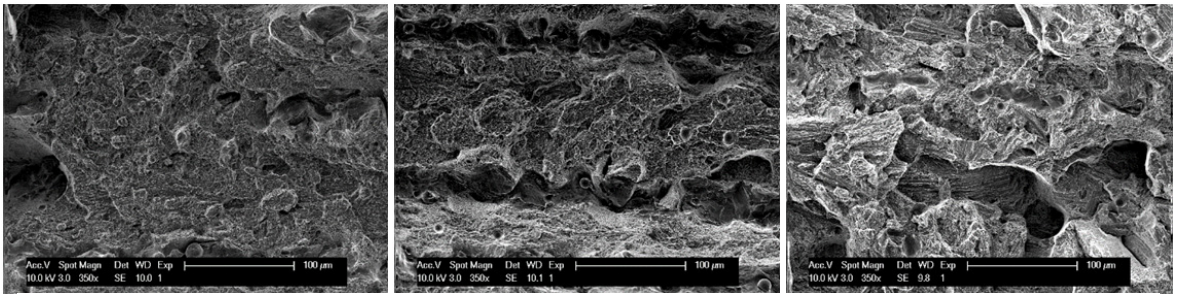

a) No preheating (ε = 4.8%) b) Preheating of 200°C (ε = 4.3%) c) Preheating of 400°C (ε = 4.3%)

Fig. 7. Fracture surfaces for samples without (a), with 200°C (b) and with 400°C (c) preheating.

4. Discussion

Significant differences in mechanical properties are found between parts build with different powder bed preheating temperatures.

Parts produced without preheating possess a martensitic structure in each newly molten layer. The XRD diffraction pattern reveals a martensitic phase as well as retained austenite. The high fraction of martensite in the top layers leads to a very high hardness of 894 ± 48$Hv_{0.5}$. Furthermore, this hard martensitic material is largely tempered during melting of subsequent layers. This is demonstrated by the hardness drop when moving away from the top surface. The big difference in microstructure between the top few layers and the rest of the part (large fraction of martensite compared to a largely tempered martensite) leads to large compressive stresses at the top of the part.

At a preheating temperature of 200°C, the microstructure is comparable to the microstructure obtained without application of preheating. The XRD diffraction pattern shows a larger fraction of retained austenite due to the less fast quenching. Slightly lower hardness and residual stress values of the top of the parts support this conclusion. Analogous to parts built without preheating, large tempering takes place when the next layers are molten, which is confirmed by the drop in hardness when moving away from the top surface. The global hardness and strength of parts produced with a preheating temperature of 200°C are lower than of parts produced without preheating. This is again due to the lower cooling rates which causes formation of more retained austenite.

For a preheating temperature of 400°C, other phenomena are observed, which indicate formation of a different microstructure. Based on the continuous cooling transformation diagram shown in Interlloy (2011), which indicates a martensitic transformation temperature of about 350°C and the martensitic transformation temperature of 300°C reported by Eser et al. (2016), the material stays above martensite transformation temperature during processing. Since production times are, depending on the run, in the range of 5-10 hours, the cct diagram suggests formation of bainite. This is a reasonable suggestion since bainite is an intermediate form between martensite and perlite. Hardness measurements of the very top of the parts indicate that hardnesses are lower for preheating of 400°C than for 200°C and no preheating because the formed bainite is not as hard as non-tempered martensite. Furthermore, the microstructure is more uniform throughout the part since the formation of bainite occurs mainly after production, during cooling down from preheating temperature to room temperature. The bcc structure found in XRD measurements in this case points towards bainite (and not to martensite). Since the bainite formed here is stronger than the largely tempered martensitic microstructure, hardness values and strength values from tensile testing are the highest for a preheating temperature of 400°C.

In additive processes such as laser cladding or selective laser melting, usually tensile stresses are formed because of the local melting and rapid solidification of the material in each subsequent layer. For H13 tool steel, this phenomenon is counteracted by the martensite formation which causes the material to locally expand, resulting in compression stresses. This is also observed here for parts made with lower preheating temperatures. When higher preheating temperatures are used, microstructural differences between the top layer and the material underneath are reduced or even non existing, which results in large tensile stresses in the top layers of the parts.

5. Conclusion

In this research, H13 tool steel parts are produced by using selective laser melting with different powder bed preheating temperatures. It was found that low preheating temperatures of up to 200°C soften the material whereas higher preheating temperatures of 400°C result in a stronger, more uniform material. Residual stresses are compressive at low preheating temperatures and gradually evolve to a tensile nature when preheating temperatures increase.

The parts obtained by using a preheating temperature of 400°C have a very homogeneous microstructure and additionally, they possess better mechanical properties than parts produced without or with lower preheating temperatures. Remarkable here is the ultimate tensile strength of the parts which is similar to conventionally produced and heat treated H13 tool steel and the hardness which is significantly higher than conventional material. This indicates that by applying preheating during the SLM-process, additional post processing can be avoided. This leads to a more time and cost efficient production process.

Acknowledgements

The research leading to these results has received funding from the KU Leuven GOA project SUMMA and from the Flemish projects SIM-ICON Expamet (IWT#120593) and SIM-SBO MultiMet (IWT#150010).

References

AlMangour, B., Grzesiak, D., Yang, J., 2016. Nanocrystalline TiC-reinforced H13 steel matrix nanocomposites fabricated by selective laser melting. Materials and Design 96, 150-161.

Cong, D., Zhou, H., Ren, Z., Zhang, Z., Zhang, H., Meng, C., Wang, C., 2014. Ther thermal fatigue resistance of H13 steel repaired by a biomimetic laser remelting process. Materials and Design 55, 597-604.

Cornier, D., Harrysson, O., West, H., 2003. Characterisation of high alloy steel produced via electron beam melting. SFF symposium. Texas. USA.

Costa, J.M., Pires, J.T.B., Antunes, F., Nobre, J.P., Borrego, L.P., 2008. Residual stresses analysis of Nd-YAG laser welded joints. Anales de Mecánica de la Fractura 25, Vol.1.

Cottam, R., Wang, J., 2014. Characterisation of microstructure and residual stress in a 3D H13 tool steel component produced by additive manufacturing. J. Mater. Res. Vol. 29, No. 17, Sep 14, 2014.

Eser, A., Broeckmann, C., Simsir, C., 2016. Multiscale modeling of tempering of AISI H13 hot-work tool steel – Part 1: Prediction of microstructure evolution and coupling with mechanical properties. Computational Materials Science 113, 280-291.

Eser, A., Broeckmann, C., Simsir, C., 2016. Multiscale modeling of tempering of AISI H13 hot-work tool steel – Part 2: Coupling predicted mechanical properties with FEM simulations. Computational Materials Science 113, 292-300.

Gu, D. D., Meiners, W., Wissenbach, K., Poprawe, R., 2012. Laser additive manufacturing of metallic components: materials, processes and mechanisms. International Materials Reviews, 57:3, 133-164.

Interlloy Pty Ltd. 2011. H13 Tool Steel (X40CrMoV5-1), retrieved from http://www.interlloy.com.au/our-products/tool-steel/h13-tool-steel-x40crmov5-1/.

Jia, Z., Liu, Y., Li, J., Liu, L., Li, H., 2015. Crack growth behavior at termal fatigue of H13 tool steel processed by laser Surface melting. International Journal of Fatigue 78, pp.61-71.

Kempen, K., Vrancken, B., Buls, S., Thijs, L., Van Humbeeck, J., Kruth, J.-P., 2014. Selective laser melting of crack-free high density M2 high speed steel parts by baseplate preheating. Journal of Manufacturing Science and Engineering, Vol. 136, 061026.

Lee, J., Jang, J., Joo, B., Son, Y., Moon, Y., 2009. Laser surface hardening of AISI H13 tool steel. Trans. Nonferrous Met. Soc. China 19, 917-920.

Maziasz, P.J., Payzant, E.A., Schliener, M.E., McHugh, K.M., 1998. Residual stresses and microstructure of H13 steel formed by combining two different direct fabrication methods. Scripta Materialia, Vol. 39, NO. 10, pp. 1471-1476.

McHugh, K.M., Lin, Y., Zhou, Y., Lavernia, E.J., 2008. Influence of cooling rate on phase formation in spray-formed H13 tool steel. Materials Science and Engineering A 477, 50-57.

Ouyang, J.H., Mei, H., Valant, M., Kovacevic, R., 2002. Application of laser-based additive manufacturing to production of tools for friction stir welding. SFF symposium. Texas. USA.

Pinkerton, A., Li, L., 2005. Direct additive laser manufacturing using gas- and water-atomised H13 tool steel powders. International Journal of Advanced Manufacturing Technology 25: 471-479.

Sander, J., Hufenbach, J., Giebeler, L., Wendronck, H., Kühn, U., Eckert, J., 2016. Microstructure and properties of FeCrMoVC tool steel produced by selective laser melting. Materials and Design 89, 335-341.

Telasang, G., Majumdar, J., Padmanabham, G., Tak, M., Manna, I., 2014. Effect of laser parameters on microstructure and hardness of laser clad and tempered AISI H13 tool steel. Surface & Coatings Technology 258, pp. 1108-1118.

Telasang, G., Majumdar, J., Padmanabham, G., Manna, I., 2014. Structure-property correlation in laser surface treated AISI H13 tool steel for improved mechanical properties. Materials Science & Engineering A 599, 255-267.

Vrancken, B., Buls, S., Kruth, J.-P., Van Humbeeck, J., 2015. Preheating of selective laser melted Ti6Al4V: Microstructure and mechanical properties. World Conference on Titanium. San Diego, CA, US.

Zhang, Z., Zhou, H., Ren, L., Tong, X., Shan, H., Cao, Y., 2007. Tensile property of H13 die steel with convex-shaped biomimetic surface. Applied Surface Science 253, 8939-8944.